Isospin effect in peripheral heavy-ion collisions at Fermi energies*

Ya-Fei Guo(郭亚飞)[1,2] Peng-Hui Chen(陈鹏辉)[1,2] Fei Niu(牛菲)[3] Zhao-Qing Feng(冯兆庆)[1,3;1)]

[1]Institute of Modern Physics, Chinese Academy of Sciences, Lanzhou 730000, China
[2]University of Chinese Academy of Sciences, Beijing 100190, China
[3]School of Physics and Optoelectronics, South China University of Technology, Guangzhou 510640, China

Abstract: The isospin effect in peripheral heavy-ion collisions was thoroughly investigated within the framework of the Lanzhou quantum molecular dynamics (LQMD) transport model. A coalescence approach was used to recognize the primary fragments formed in nucleus-nucleus collisions. The secondary decay process of these fragments was described using the statistical code GEMINI. The production mechanism and isospin effect of the projectile-like and target-like fragments were analyzed using the combined approach. It was found that the isospin migration from the high-isospin density to the low-density matter occurred in the neutron-rich nuclear reactions, i.e., ^{48}Ca+^{208}Pb, ^{86}Kr+^{48}Ca/^{208}Pb/^{124}Sn, ^{136}Xe+^{208}Pb, ^{124}Sn+^{124}Sn, and ^{136}Xe+^{136}Xe. A hard symmetry energy was available for creating the neutron-rich fragments, particularly in the medium-mass region. The isospin effect of the neutron-to-proton (n/p) ratio of the complex fragments was reduced when the secondary decay process was included. However, a soft symmetry energy enhanced the n/p ratio of the light particles, particularly at kinetic energies greater than 15 MeV/nucleon.

Keywords: symmetry energy, nuclear fragmentation reaction, neutron-rich nuclei, LQMD transport model

PACS: 21.65.Ef, 24.10.Lx, 25.75.-q **DOI:** 10.1088/1674-1137/42/12/124106

1 Introduction

Over the past several decades, the quasi-fission or fast fission dynamics of massive nuclear reactions have attracted much attention in both experimental and theoretical studies [1–4]. The characteristics of quasi-fission reactions have been extensively studied, particularly to understand the formation mechanism of superheavy nuclei during low-energy nuclear collisions. The composite system in quasi-fission reactions persists during the long time scale of the relative energy dissipation and nucleon transfer, in which the isospin dependent nucleon-nucleon potential dominates the fragment formation. The symmetry energy as an ingredient of the nuclear equation of state (EOS) in the domain of sub-saturation densities is important to understand the structure of a weakly bound nucleus, nuclear liquid-gas phase transition, nuclear boundary of the neutron-rich nuclide, etc. [5–11]. A soft symmetry energy in the domain of sub-saturation densities has been extracted from the different observables during Fermi-energy (10-100 MeV/nucleon) heavy-ion collisions [12–16]. Different mechanisms might coexist and be correlated during heavy-ion collisions at the Fermi energies[17], such as projectile or target fragmentation, neck dynamics and fragment formation, the pre-equilibrium emission of light clusters (complex particles), the fission of heavy fragments, and multifragmentation, in which the isospin dependent nucleon-nucleon potential dominates the dynamical processes. Recently, the isospin effects of the intermediate mass fragments (IMFs) from the neck fragmentation were thoroughly investigated [18–20]. The neutron-enrichment phenomenon in the neck region was observed for the first time by the CHIMERA collaboration [19].

On the other hand, the neutron-to-proton ratios of the projectile-like or target-like fragments are also related to the isospin dependent potential. In this study, we investigated the isospin dynamics of the fragment formation and decay modes in peripheral heavy-ion collisions within the Lanzhou quantum molecular dynamics (LQMD) transport model. In Sec. 2 we provide a brief description of the LQMD model. The isospin dissipation dynamics and symmetry energy effect are discussed in Sec. 3. A summary and perspective on the possible measurements are presented in Sec. 4.

2 Model description

The LQMD transport model was developed to understand the isospin dynamics during medium- and high-

Received 22 July 2018, Revised 20 September 2018, Published online 25 October 2018

∗ Supported by the National Natural Science Foundation of China (11722546, 11675226) and the Talent Program of South China University of Technology (K5180470)

1) E-mail: fengzhq@scut.edu.cn (corresponding author)

energy heavy-ion collisions. It considers the issues of the symmetry energy at subnormal and suprasaturation densities, in-medium nucleon-nucleon (NN) cross sections, isospin- and momentum-dependent NN potential, isospin effects on particle production and transportation, etc. [21–24]. All of the possible reaction channels of the charge-exchange, elastic, and inelastic scatterings are implemented in the model by distinguishing the isospin effects in hadron-hadron collisions. The temporal evolutions of the baryons (nucleons and resonances) and mesons in the colliding system under the self-consistently generated mean-field are described by Hamilton's equations of motion. The Hamiltonian is constructed with the Skyrme-type interaction, which consists of the relativistic energy and effective interaction potential. We do not take into account the momentum-dependent potential in the Fermi-energy and near-barrier nuclear collisions for stabilizing the initial nucleus. However, the momentum-dependent interaction has to be included in the high-energy heavy-ion collisions, which reduces the effective nucleon mass in a nuclear medium.

The local potential can be written with the energy-density functional as $U_{\rm loc}=\int V_{\rm loc}(\rho(\boldsymbol{r}))\mathrm{d}\boldsymbol{r}$. The energy-density functional is expressed by the following:

$$V_{\rm loc}(\rho)= \frac{\alpha}{2}\frac{\rho^2}{\rho_0}+\frac{\beta}{1+\gamma}\frac{\rho^{1+\gamma}}{\rho_0^{\gamma}}+E_{\rm sym}^{\rm loc}(\rho)\rho\delta^2 +\frac{g_{\rm sur}}{2\rho_0}(\nabla\rho)^2+\frac{g_{\rm sur}^{\rm iso}}{2\rho_0}[\nabla(\rho_{\rm n}-\rho_{\rm p})]^2, \quad (1)$$

where $\rho_{\rm n}$, $\rho_{\rm p}$, and $\rho=\rho_{\rm n}+\rho_{\rm p}$ are the neutron, proton, and total densities, respectively, and $\delta=(\rho_{\rm n}-\rho_{\rm p})/(\rho_{\rm n}+\rho_{\rm p})$ represents the isospin asymmetry. The parameters α, β, γ, $g_{\rm sur}$ $g_{\rm sur}^{\rm iso}$, and ρ_0 are taken to be -226.5 MeV, 173.7 MeV, 1.309, 23 MeV fm^2, -2.7 MeV fm^2, and 0.16 fm^{-3}, respectively. These parameters lead to the compression modulus of $K=230$ MeV for isospin symmetric nuclear matter at the saturation density. $E_{\rm sym}^{\rm loc}$ is the local potential of the symmetry energy given by the following:

$$E_{\rm sym}^{\rm loc}(\rho)=\frac{1}{2}C_{\rm sym}(\rho/\rho_0)^{\gamma_s} \quad (2)$$

where the coefficients γ_s=0.5, 1, and 2 correspond to the soft, linear, and hard symmetry energies, respectively. The value of $C_{\rm sym}$=38 MeV results in a symmetry energy of 31.5 MeV at the normal nuclear density.

In low-energy heavy-ion collisions, the fermionic nature of the nucleons and NN elastic scattering dominate the nuclear dynamics and fragment formation. The Pauli blocking in NN collisions is treated differently in the various transport models [25]. The purpose is to reduce the collision probability for the quantal many-body system. In the LQMD model, the Pauli blocking in NN collisions is embodied by the blocking probability $b_{ij}=1-(1-f_i)(1-f_j)$ for two colliding nucleons i and j compared with a random number. The isospin effect is included in the evaluation of the occupation probability as follows:

$$f_i = \frac{32\pi^2}{9h^3}\sum_{i\neq k,\tau_i=\tau_k}(\triangle r_{ik})^2(3R_0-\triangle r_{ik}) \times(\triangle p_{ik})^2(3P_0-\triangle p_{ik}). \quad (3)$$

Here, $r_{ik}=|\boldsymbol{r}_i-\boldsymbol{r}_k|$ and $p_{ik}=|\boldsymbol{p}_i-\boldsymbol{p}_k|$ represent the relative distances of two nucleons in the coordinate and momentum spaces, respectively. The sum satisfies the conditions of $r_{ik}<2R_0$ and $p_{ik}<2P_0$, with $R_0=3.367$ fm and $P_0=112.5$ MeV/c. It should be noted that the overlap of a hard sphere in the phase space is assumed by $16\pi^2R_0^3P_0^3/9=h^3/2$. The cross section of the NN elastic scattering is obtained by fitting the available experimental data to the wide energy region [26].

The nuclear dynamics of the Fermi-energy heavy-ion collisions is described by the LQMD model. The primary fragments are constructed in the phase space with a coalescence model, in which nucleons at freeze-out are considered to belong to one cluster with a relative momentum that is smaller than P_0 and relative distance that is smaller than R_0 (here P_0 = 200 MeV/c and R_0 = 3 fm) [20]. The primary fragments are highly excited, and the de-excitation of the fragments is described within the GEMINI code [27].

3 Results and discussion

The phase-space structure of the fragments produced in heavy-ion collisions provides the correlation and fluctuation of the nuclear dynamics in the dissipation of the relative motion energy, nucleon transfer, and isospin density. The yields of the primary fragments in the peripheral HICs almost exhibit a symmetric distribution in the projectile-like fragments (PLFs) or target-like fragments (TLFs) because of the same stripping and pick-up reaction rates. The fragment spectra are influenced by both the dynamics mechanism and structure quantities. The proton and neutron drifts in the different density regions are driven by the mean-field potential in the nuclear medium. Figure 1 shows the fragment distributions in the reactions of ^{86}Kr+^{48}Ca/^{208}Pb and ^{136}Xe+^{136}Xe at an incident energy of 20 MeV/nucleon during peripheral collisions with impact parameters of 7–9 fm, 8–10 fm, and 8–10 fm, respectively. The parallel velocity $V_{\rm PAR}$ is evaluated along the beam direction in the center of mass frame, where positive (negative) values correspond to the PLFs (TLFs). It is obvious that numerous fragments are created in the vicinity of a projectile or target velocity. The intermediate mass fragments (IMFs) are mainly produced during the nuclear fragmentation reactions. The N/Z ratio of IMFs from the neck fragmentation during Fermi-energy heavy-ion collisions is enhanced by the isospin migration and has been investigated to extract

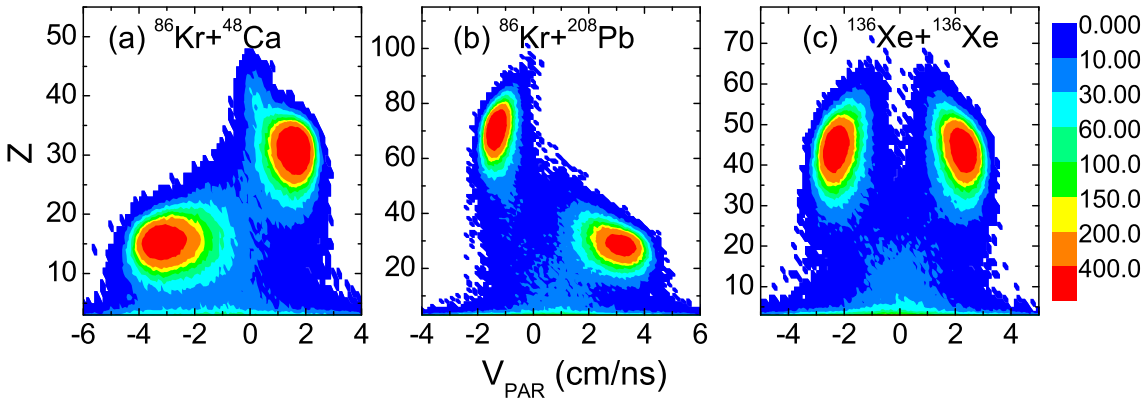

Fig. 1. (color online) Fragment yields produced in collisions of ^{86}Kr+^{48}Ca, ^{86}Kr+^{208}Pb, and ^{136}Xe+^{136}Xe at incident energy of 20 MeV/nucleon as functions of atomic number Z and parallel velocity $V_{\rm PAR}$.

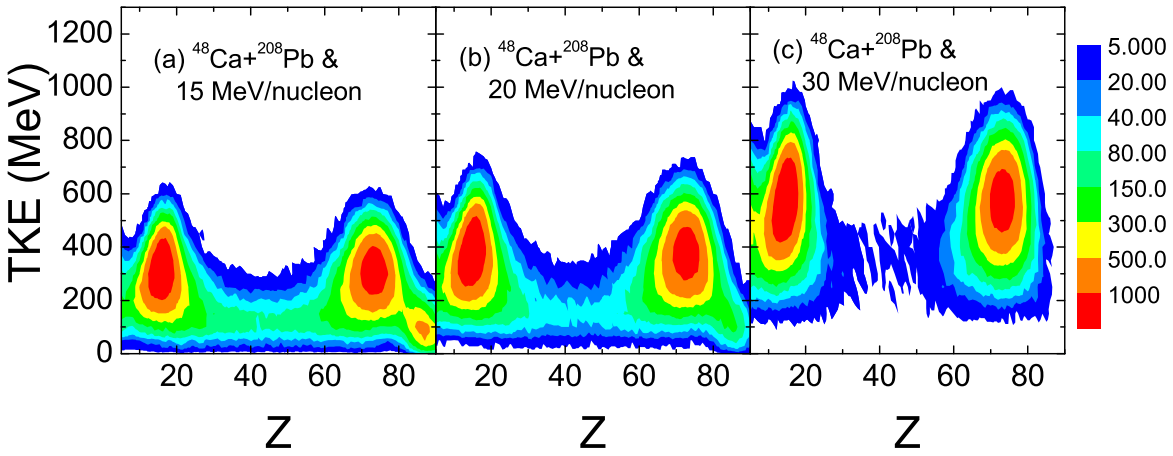

Fig. 2. (color online) Total kinetic energy spectra during ^{48}Ca+^{208}Pb reaction at energies of 15, 20, and 30 MeV/nucleon.

the subnormal density symmetry energy [19, 20].

Fig. 2 shows the total kinetic energy (TKE) distribution of the primary fragments during the reaction of ^{48}Ca+^{208}Pb within the collision centrality of 8–10 fm. We count the kinetic energies from the bound fragments, excluding the free nucleons. The fast free nucleons take a portion of the energies from the colliding system, which decreases the TKE in comparison to the incident energy. It is obvious that the TKE spectra exhibit a symmetric structure. The multinucleon transfer mechanism is available for creating medium-mass fragments in the region where the charged numbers are Z = 30–60. The dissipations of the relative motion energy and nucleon transfer are more pronounced with a decrease in the incident energy because of the greater relaxation time. The difference in the neutron and proton chemical potentials influences the neutron enrichment of the fragments. The isospin effect is expected to appear from the distributions of the PLFs and TLFs during near-barrier nuclear collisions.

The isospin dynamics of the fast nucleons and light complex particles produced in Fermi-energy heavy-ion collisions has been investigated to determine the symmetry energy at subsaturation densities and the isospin splitting of the nucleon effective mass in nuclear matter [28]. The pre-equilibrium nucleon emission in an isotopic reaction system was measured at the National Superconducting Cyclotron Laboratory (Michigan State University, East Lansing, MI, USA) [29]. The production of fragments can be calculated using the combined approach of the LQMD transport model for the primary fragments and the GEMINI statistical decay code for the de-excitation process [27]. The de-excitation of fragments with a charge number $Z>6$ is considered. Only light fragments from the pre-equilibrium emission in nuclear collisions are counted. The excitation energy with $Z>6$ is evaluated using the binding energy difference between the primary fragments and ground state eval-

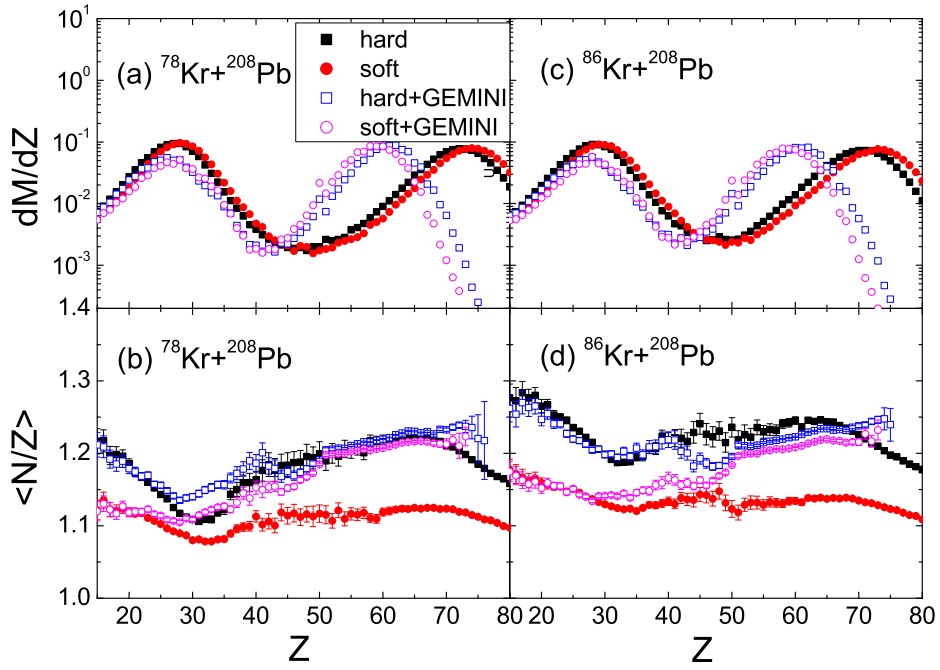

Fig. 3. (color online) Total multiplicities and $\langle N/Z\rangle$ ratio as function of charged numbers of fragments produced in reactions of ^{78,86}Kr+^{208}Pb at 20 MeV/nucleon.

uated using the liquid drop model. Figure 3 shows the total multiplicities and average neutron/proton ratios ($\langle N/Z\rangle$)of the heavy fragments produced during peripheral collisions of ^{78,86}Kr + ^{208}Pb at a beam energy of 20 MeV/nucleon with the impact parameters of 8–10 fm. The isospin effect is weakened by the decay process, particularly in the heavy mass domain, because of the larger excitation energy. This is because the stability of a single nucleus at the time evolution is weakly influenced by the stiffness of the symmetry energy in the LQMD model. The conclusions are different from the calculations of the ImQMD05 code [30]. A hard symmetry energy has been found to be favorable for the formation of neutron-rich isotopes. However, the yields are weakly influenced by the stiffness of the symmetry energy. The de-excitation of the primary fragments moves the spectra to the light mass region. It has been found that the peripheral nucleus-nucleus collisions have the advantage of creating neutron-rich isotopes [31]. Figure 4 shows a comparison of the effects of the different symmetry energies on the fragment distribution in the symmetric reaction of ^{136}Xe+^{136}Xe at an incident energy of 20 MeV/nucleon, with the impact parameters of 8-10 fm. The "inverse quasi-fission process" leads to the one-bump structure. Moreover, the fragment yields are almost independent of the stiffness of the symmetry energy. However, the $\langle N/Z\rangle$ ratios of the isotopic fragments exhibit an obvious isospin effect in the wide mass region. These conclusions were helpful in extracting the symmetry energy from the quasi-fission fragments at the INFN-LNS Superconducting Cyclotron of Catania

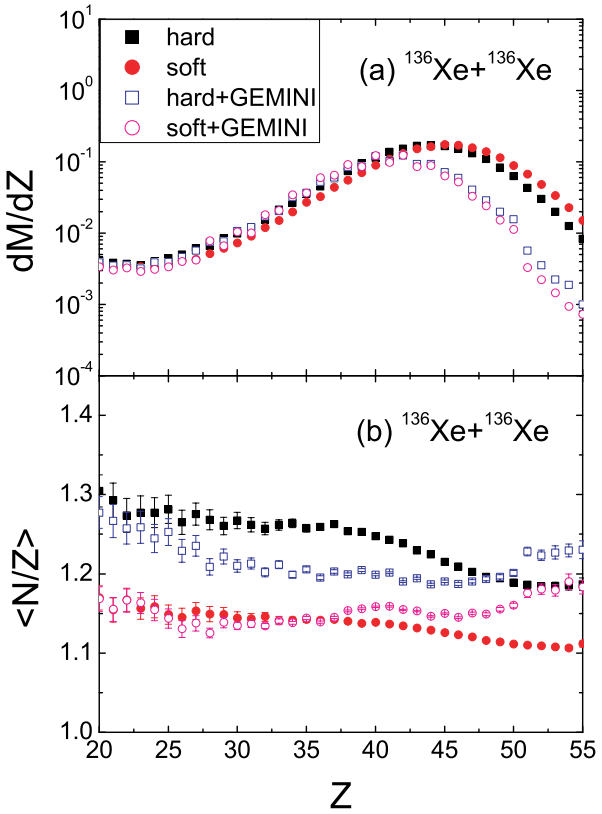

Fig. 4. (color online) Just as in Fig. 3, but for symmetric reaction ^{136}Xe+^{136}Xe at 20 MeV/nucleon with hard and soft symmetry energies.

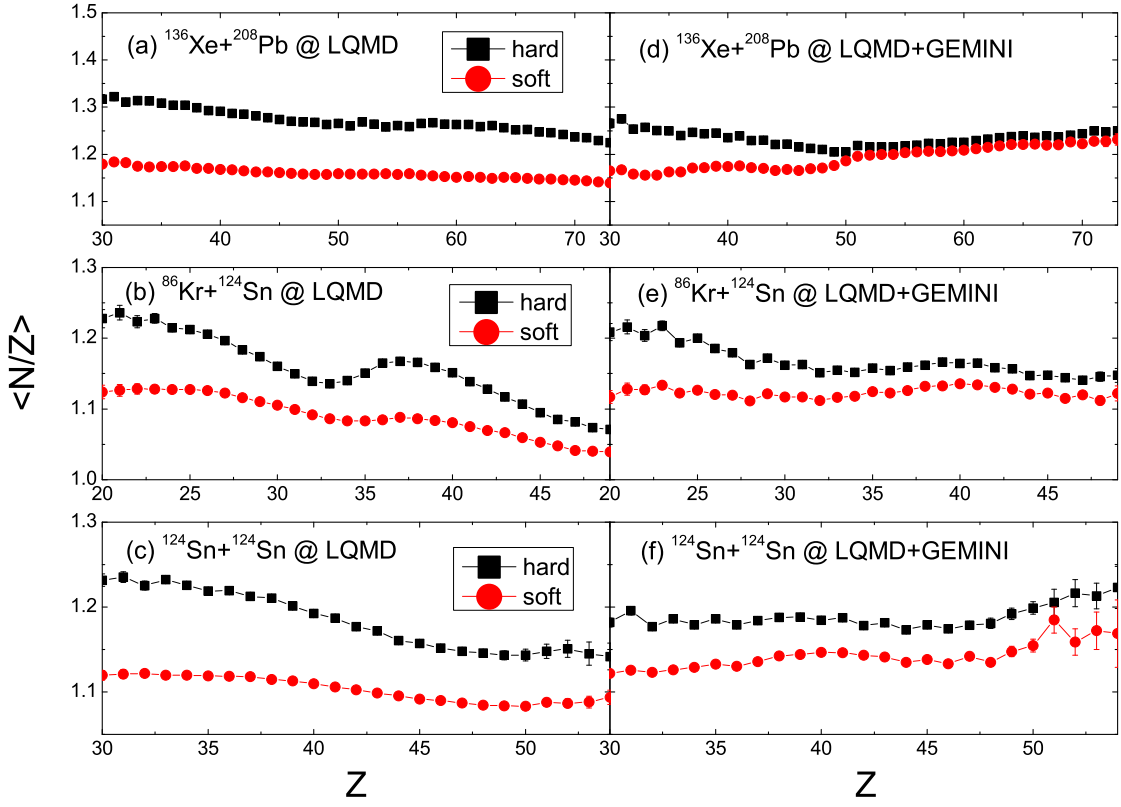

Fig. 5. (color online) Comparison of $\langle N/Z\rangle$ ratios of primary (left panels) and secondary (right panels) fragments with hard and soft symmetry energies in reactions of ^{136}Xe+^{208}Pb, ^{86}Kr+^{124}Sn, and ^{124}Sn+^{124}Sn at energy of 20 MeV/nucleon.

(Italy) [32].

A systematic comparison of the $\langle N/Z\rangle$ ratios of the primary and secondary fragments from different reaction systems is shown in Fig. 5. The isospin effect is obvious in the spectra of the primary fragments, which directly provides mean-field information. The hard symmetry energy results in larger $\langle N/Z\rangle$ ratios for the fragment formation because of the weaker repulsive force for neutrons in the neutron-rich matter, which is available for the neutron-rich isotope formation during peripheral heavy-ion collisions. To realize the cold fragments observed in experiments, we implemented the GEMINI code for the primary fragments. The isospin effect is weakened by the de-excitation process, particularly in the heavy-mass domain. The neutron-rich isotopes have smaller neutron separation energies. The statistical decay reduces the $\langle N/Z\rangle$ ratio with the hard symmetry energy. However, the primary proton-rich fragments formed with the soft symmetry energy might be decayed by the proton or neutron emission. Figure 6 shows the kinetic energy spectra of the neutron/proton ratios from the "gas-phase" fragments (nucleons, hydrogen, and helium isotopes) produced in collisions of ^{136}Xe+^{208}Pb, ^{86}Kr+^{124}Sn, and ^{124}Sn+^{124}Sn with the same impact parameters of 8–10 fm at an energy of 20 MeV/nucleon. The symmetry energy effect is more pronounced for the neutron-rich system. The bump structure of the primary fragments at an energy of approximately 15 MeV/nucleon is caused by the competition of the free nucleons and light fragments with the n/p ratios. The light fragments with $Z\leq 2$ are mainly produced at a low kinetic energy and have smaller n/p ratios in comparison to the free nucleons. At kinetic energies greater than 30 MeV/nucleon, the n/p ratios are mainly contributed from the free nucleons. After a turning point at approximately the Fermi energy (36 MeV), the n/p ratios increase with the kinetic energy. The structure of the spectra is determined by the Coulomb interaction competition between the charged particles and symmetry potential, which enhances the proton and neutron yields, respectively [20]. The difference between the hard (γ_s=2) and soft (γ_s=0.5) symmetry energies is obvious in the entire energy range. In contrast to the trend for the $\langle N/Z\rangle$ ratio of the IMFs and heavy fragments, the soft symmetry energy enhances the yield ratios because of the greater repulsive force for neutrons in the dynamical evolution. It should be noted that the $\langle N/Z\rangle$

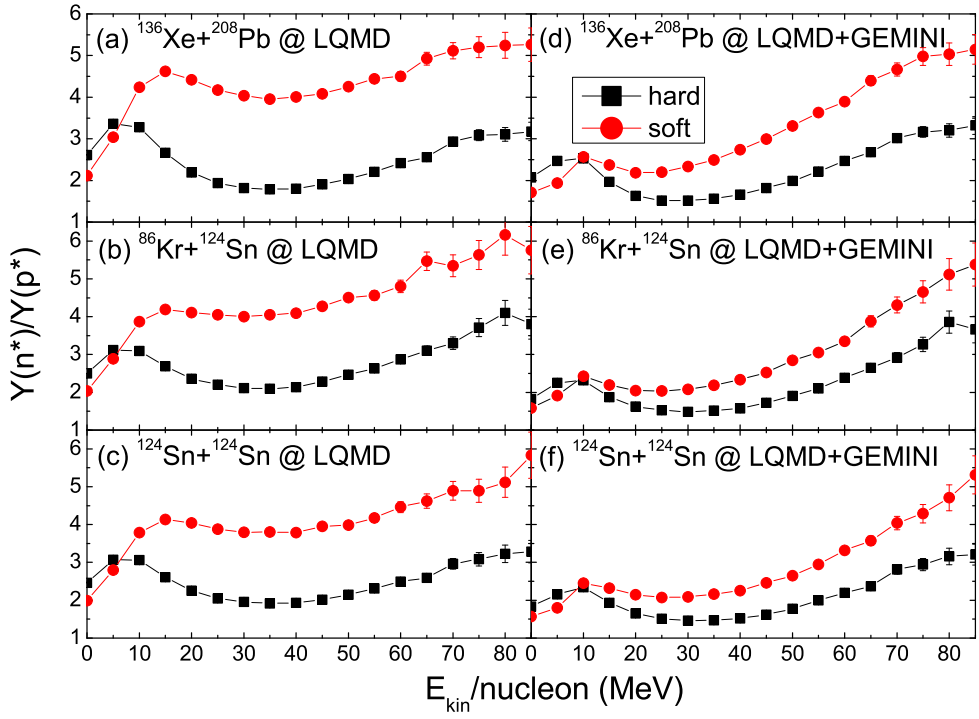

Fig. 6. (color online) Just as in Fig. 5, but for kinetic energy spectra from yields of gas-phase particles (nucleons, hydrogen and helium isotopes).

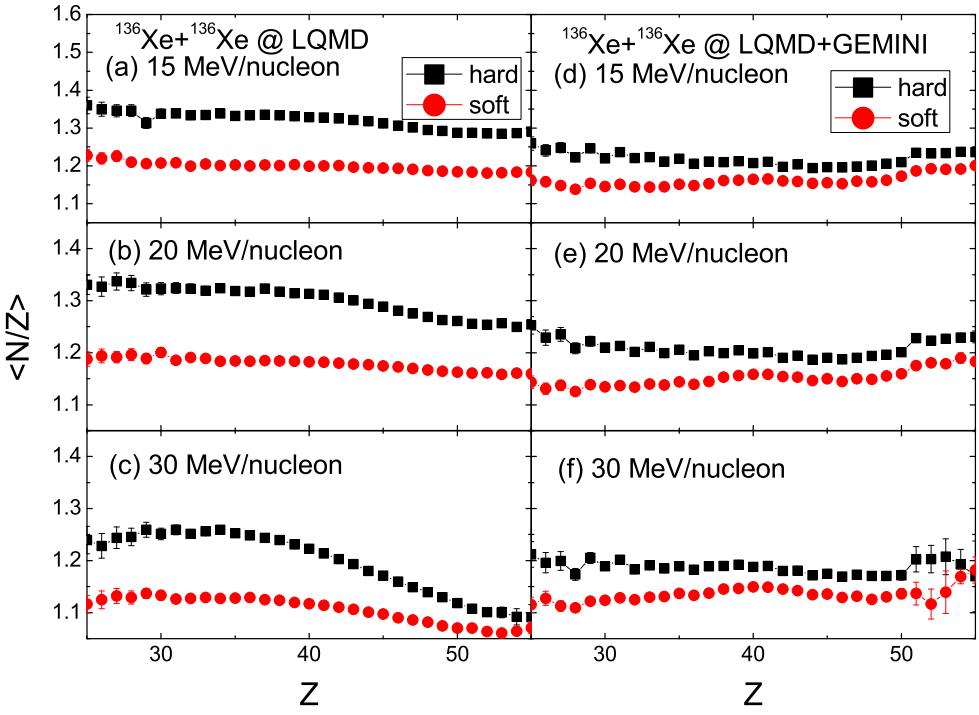

Fig. 7. (color online) Incident energy dependence of $\langle N/Z\rangle$ ratio in reaction of ^{136}Xe + ^{136}Xe.

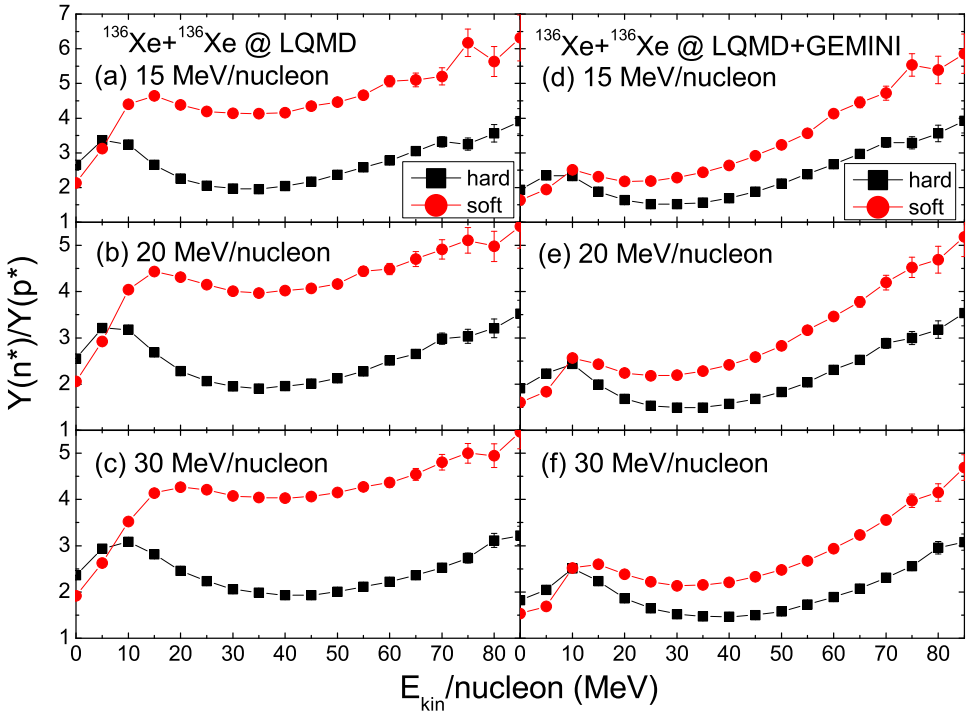

Fig. 8. (color online) "Gas-phase" n/p ratio as function of kinetic energy in collisions of ^{136}Xe + ^{136}Xe at beam energies of 15, 20, and 30 MeV/nucleon.

ratio of the fragments is below the β-stability line because more neutrons are unbound and emitted with the mean-field potential. Large n/p ratios are obtained in the gas phase.

The isospin dissipation during peripheral heavy-ion collisions is related to the incident energy. The composite system maintains a greater temporal relaxation with a decrease in the energy, in which the isospin-dependent single-particle potential impacts the nucleon dynamics and fragment formation. Figure 7 shows a comparison of the effects of the different energy values on the $\langle N/Z\rangle$ ratios of the fragments produced in the ^{136}Xe + ^{136}Xe reaction. A large $\langle N/Z\rangle$ ratio is obtained with the hard symmetry energy at 15 MeV/nucleon. The isospin effect is still pronounced after including the statistical decay. The dependence of the kinetic energy spectra of the "gas-phase" n/p ratio on the incident energy is small, as shown in Fig. 8. The correlation measurements of the $\langle N/Z\rangle$ ratios from the heavy fragments and the n/p yield ratios from the "gas-phase" particles are helpful in constraining the symmetry energy at subsaturation densities, as well as in the synthesis of new neutron-rich isotopes. The multinucleon transfer reaction during Fermi-energy heavy-ion collisions was investigated using the improved quantum molecular dynamics (ImQMD) model. A narrower angular distribution of PLFs and TLFs was obtained in comparison with that of low-energy nuclear collisions [33].

4 Conclusions

Using the LQMD transport model, we investigated the isospin dynamics of peripheral heavy-ion collisions at Fermi energies. The n/p spectra from the gas-phase particles, PLFs, and TLFs were thoroughly analyzed. The average n/p ratios of the IMFs and heavy fragments were sensitive to the stiffness of the symmetry energy because of the existence of an isospin density gradient in dissipative collisions. The hard symmetry energy was available for producing neutron-rich fragments. However, the isospin effect was reduced after implementing the statistical decay because of binary fission and light particle evaporation. The larger n/p yield ratios of the "gas phase" particles were obtained with the soft symmetry energy because of the repulsive interaction enforced on neutrons in the region of sub-saturation densities. Further experiments should be conducted to extract the subnormal symmetry energy from the medium fragments.

References

1 M. G. Itkis, E. Vardaci, I. M. Itkis et al, Nucl. Phys. A, **944**: 204 (2015)
2 V. Zagrebaev and W. Greiner, J. Phys. G, **34**: 1 (2007)
3 Z. Q. Feng, G. M. Jin, J. Q. Li, and W. Scheid, Nucl. Phys. A, **816**: 33 (2009)
4 Y. Aritomo, K. Hagino, K. Nishio, and S. Chiba, Phys. Rev. C, **85**: 044614 (2012)
5 P. Chomaz, M. Colonna, and J. Randrup, Phys. Rep., **389**: 263 (2004)
6 M. Colonna, M. Di Toro, A. Guarnera, V. Latora, and A. Smerzi, Phys. Lett. B, **307**: 273 (1993); M. Colonna, M. Di Toro, and A. Guarnera, Nucl. Phys. A, **580**: 312 (1994)
7 J. Pochatlzalla et al, Phys. Rev. Lett., **75**: 1040 (1995)
8 Y. G. Ma, Phys. Rev. Lett., **83**: 3617 (1999)
9 Y. Zhang, Z. Li, Phys. Rev. C, **71**: 024604 (2005)
10 X. G. Deng, Y. G. Ma, Nucl. Sci. Tech., **28**: 82 (2017)
11 N. B. Zhang, B. J. Cai, B. A. Li et al, Nucl. Sci. Tech., **28**: 181 (2017)
12 V. Baran, M. Colonna, V. Greco, M. Di Toro, Phys. Rep., **410**: 335 (2005)
13 L. W. Chen, C. M. Ko, B. A. Li, Phys. Rev. Lett., **94**: 032701 (2005)
14 B. A. Li, L. W. Chen, C. M. Ko, Phys. Rep., **464**: 113 (2008)
15 Z. Y. Sun, M. B. Tsang, W. G. Lynch et al, Phys. Rev. C, **82**: 051603(R) (2010)
16 Z. Kohley et al, Phys. Rev. C, **83**: 044601 (2011)
17 R. Ogul, N. Buyukcizmeci, A. Ergunet al, Nucl. Sci. Tech., **28**: 18 (2017)
18 E. De Filippo, A. Pagano, P. Russotto et al, Phys. Rev. C, **86**: 014610 (2012)
19 E. De Filippo and A. Pagano, Eur. Phys. J. A , **50**: 32 (2014); P. Russotto et al, Phys. Rev. C, **91**: 014610 (2015)
20 Z. Q. Feng, Phys. Rev. C, **94**: 014609 (2016)
21 Z. Q. Feng, Phys. Rev. C, **84**: 024610 (2011)
22 Z. Q. Feng and H. Lenske, Phys. Rev. C 89, 044617 (2014); Z. Q. Feng, **93**: 041601(R) (2016)
23 Z. Q. Feng, W. J. Xie, P. H. Chen, J. Chen, and G. M. Jin, Phys. Rev. C, **92**: 044604 (2015)
24 Z. Q. Feng, Nucl. Sci. Tech., **29**: 40 (2018); J. Chen, Z. Q. Feng, and J. S. Wang, Nucl. Sci. Tech., **27**: 73 (2016)
25 Y. X. Zhang et al, Phys. Rev. C, **97**: 034625 (2018)
26 Z. Q. Feng and G. M. Jin, Chin. Phys. Lett., **26**: 062501 (2009)
27 R. J. Charity, M. A. McMahan, G. J. Wozniak et al, Nucl. Phys. A, **483**: 371 (1988)
28 Y. F. Guo, P. H. Chen, F. Niu et al, Chin. Phys. C, **41**: 104104 (2017)
29 D. D. S. Coupland, M. Youngs, Z. Chajecki et al, Phys. Rev. C, **94**: 011601(R) (2016)
30 Y. Zhang, D. D. S. Coupland, P. Danielewicz et al, Phys. Rev. C, **85**: 024602 (2012)
31 T. I. Mikhailova, B. Erdemchimeg, A. G. Artyukh, G. Kaminski, Yu. M. Sereda, M. Colonna, M. Di Toro, and H. H. Wolter, Bull. Russ. Aca. Sci. (Physics), **75**: 1511 (2011) DOI: 10.3103/S1062873811110190
32 B. Gnoffo et al, Journal of Physics: Conf. Series, **863**: 012062 (2017)
33 H. Yao and N. Wang, Phys. Rev. C, **95**: 014607 (2017)